

Fast-Poly: A Fast Polyhedral Framework For 3D Multi-Object Tracking

Xiaoyu Li[†], Dedong Liu[†], Lijun Zhao^{*}, Yitao Wu[†], Xian Wu[†], Jinghan Gao

Abstract—3D Multi-Object Tracking (MOT) captures stable and comprehensive motion states of surrounding obstacles, essential for robotic perception. However, current 3D trackers face issues with accuracy and latency consistency. In this paper, we propose Fast-Poly, a fast and effective filter-based method for 3D MOT. Building upon our previous work Poly-MOT, Fast-Poly addresses object rotational anisotropy in 3D space, enhances local computation densification, and leverages parallelization technique, improving inference speed and precision. Fast-Poly is extensively tested on two large-scale tracking benchmarks with Python implementation. On the nuScenes dataset, Fast-Poly achieves new state-of-the-art performance with 75.8% AMOTA among all methods and can run at 34.2 FPS on a personal CPU. On the Waymo dataset, Fast-Poly exhibits competitive accuracy with 63.6% MOTA and impressive inference speed (35.5 FPS). The source code is publicly available at <https://github.com/lixiaoyu2000/FastPoly>.

Index Terms—Multi-Object Tracking, Real-Time Efficiency, 3D Perception

I. INTRODUCTION

3D MULTI-OBJECT TRACKING filters and recalls obstacle observations, being a crucial component in autonomous driving and robot perception systems. Recent advances in 3D MOT can be attributed to the success of the Tracking-By-Detection (TBD) framework¹. Despite the advancements, these filter-based works [1]–[7] currently suffer from the consistency of accuracy and latency on large-scale datasets (nuScenes [8], Waymo [9], etc.), as shown in Fig. 1. Specifically, these datasets mainly bring the proliferation of tracking agents, magnifying four primary shortcomings of filter-based methods:

- **Object is rotated in 3D space.** Geometry-based metrics (IoU [10], [11], GIoU [1], [2], [4]) provide high interpretability and accurately capture inter-object affinity, are widely utilized. However, according to statistics in Table II, 3D object rotation leads to time-consuming polygon intersection and convex hull solution steps in these metrics. Some works [3], [12], [13] employ custom Euclidean distance to reduce overhead, but accuracy is lost due to the lack of spatial relationship considerations.
- **The tracking pipeline is from a global perspective.** Modeling global object similarity for pre-processing and association is a common practice in the field [1]–[4], [10]–[13]. However, inter-observation redundancy and trajectory-observation correlation are only feasible in a

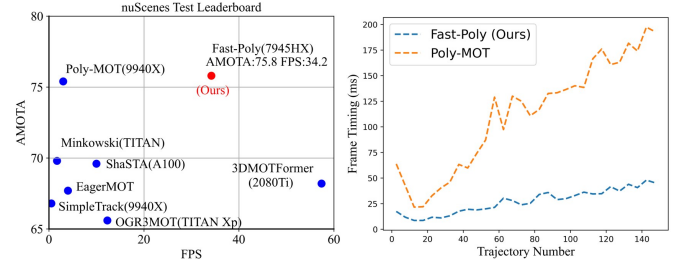


Fig. 1: **Left:** The comparison of the accuracy and latency between our method and advanced trackers on **nuScenes test leaderboard**. The closer to the top right, the better the performance. Fast-Poly also exhibits superior performance on the **Waymo test leaderboard** with 63.6% MOTA and 35.5 FPS. **Right:** The time consumption curve of average frame timing with the objects increasing between our proposed Fast-Poly and baseline method Poly-MOT on nuScenes val set.

limited local space, leading to numerous invalid computations. [1], [2], [4] emphasize restricting false positive (FP) agents from influencing cost computations. [1] also applies multiple criteria to avoid distinct categories matching. Despite these efforts, the fact that *distant objects are unrelated* is widely ignored.

- **Matrix calculations in filters are heavy.** Trajectories typically represented as high-dimensional vectors [1]–[4], [10]–[13]. Nevertheless, integrating time-invariant states in the Kalman Filter (KF) leads to redundant computations involving zeros. [14] accelerates 2D position estimation through a priori split calculation and CUDA operator. However, in 3D MOT, the abundance of states and non-linear motion models [1] make a similar matrix-to-quadratic form transformation challenging. Furthermore, rigid count-based lifecycle management hinders real-time performance due to matrix operations applied to all active tracklets, including the coasted FP tracklets.
- **The TBD framework is serial logic inherently.** Existing methods rely on a module-by-module program execution order due to the extensive fusion calculations between observations and tracklets within the TBD framework. This conventional view overlooks the potential for localized parallel processing, hindering efficiency.

Towards these issues, we propose Fast-Poly, a fast and effective polyhedral framework for 3D MOT. Specifically, to eliminate the object rotation impact, we introduce an elegant solution: Align rotated objects and then employ 2D-like parallel IoU operations for accelerated similarity calculations. To avoid invalid global affinity computations, we introduce

[†]: These authors contributed equally to this work. ^{*}: Corresponding author. All authors are with State Key Laboratory of Robotics and System, Harbin Institute of Technology, Harbin 150006, China.

¹Top 5 methods on **nuScenes** are all adhere to the TBD framework.

the voxel mask to calculate valuable costs quickly based on coarse-to-fine criteria. To minimize the KF burden, we first incorporate a lightweight filter to decouple and manage time-invariant states, streamlining the trajectory vectors. Additionally, we propose a confidence-count mixed lifecycle strategy to flexibly terminate the trajectory, mitigating FP tracking agents in the maintenance list. As a practical solution, we parallelize pre-processing and motion prediction based on their independent relationships, alleviating the serial bottleneck.

Fast-Poly is learning-free and can perform fast, accurate tracking with limited resources (only CPU). Fast-Poly builds upon our previous work Poly-MOT [1], an advanced tracker optimized for multi-category scenes. With the Python implementation, Fast-Poly is fully assessed on two autonomous driving datasets (nuScenes [8], Waymo [9]). **On nuScenes, Fast-Poly establishes a new state-of-the-art with 75.8% AMOTA and 34.2 FPS among all methods**, accompanied by a $5\times$ faster inference speed than baseline. On Waymo, Fast-Poly attains competitive performance with 63.6% MOTA and impressive speed (35.5 FPS). Our main contributions include:

- We propose Fast-Poly, a filter-based 3D MOT method that combines high real-time performance with outperform accuracy across two large-scale autonomous driving datasets (nuScenes [8], Waymo [9]).
- We leverage rotated object alignment, local computation densification, and module parallelization techniques to solve the real-time dilemma of filter-based methods while improving accuracy.
- We achieve state-of-the-art tracking performance on the nuScenes test leaderboard among all methods with 75.8% AMOTA and 34.2 FPS.
- Our code is made publicly available, aiming to serve as a strong baseline for the community.

II. RELATED WORK

A. 3D Multi-Object Tracking

Current 3D MOT [1]–[7], [10]–[13], [15]–[20] benefits from advancements in 2D MOT [14], [21]–[24] and 3D detection [20], [25]–[30]. AB3DMOT [10] pioneers the expansion of the TBD framework into 3D space, introducing a simple yet effective baseline. Poly-MOT [1] proposes category-specific ideas to introduce a strong tracker based on multiple non-linear models and similarity metrics, achieving SOTA performance on nuScenes. With Neural Network (NN) and a post-processing manner, some methods [5]–[7], [16] utilize the features output by the pre-trained backbone [20] to regress the affinity or even the tracking confidence [6]. Leveraging the occlusion robustness of LiDAR and the far-sightedness of cameras, EagerMOT [3] performs a detection-level fusion to combine 2D and 3D detectors. CAMO-MOT [2] introduces an occlusion head to classify the visual occlusion status and implements a confidence-involved LiDAR association. JMOT [31] and mmMOT [32] develop a feature-level fusion multi-modal tracker, generating detections and association based on the Joint Detection and Tracking (JDT) framework. Being economical and an end-to-end pipeline, camera-only trackers [18], [19] based on Bird’s-Eye View (BEV)

representation receive attention and applications. Following the Tracking-By-Attention (TBA) framework, these trackers implement spatial-temporal modeling based on self/cross-attention and implicitly learn trajectory motion in a self-refinement paradigm. The trade-off between computational overhead, real-time performance, and tracking accuracy stands as the primary research direction in the current landscape.

B. Tracking-By-Detection

Core Idea. Taking advanced detection results as input, tracking is handled independently on the tracker-end entirely in a post-processing manner. The TBD framework features a well-established pipeline, dividing 3D MOT into four components: pre-processing, estimation, association, and lifecycle.

Pre-processing. This module recalls high-quality observations from raw detections based on spatial information between detections (Non-Maximum Suppression [1], [2], [4], NMS) or confidence (Score Filter [1], [2], SF). However, the global perspective inherent in the process leads to redundant computations. In contrast, our method employs the voxel mask, effectively bypassing these calculations.

Estimation. This module utilizes filters (Linear Kalman Filter [2]–[4], [10]–[13], Extended Kalman Filter [1], Point Filter [15], [20], etc.), along with motion models, to perform two functions: (1) Predict the alive tracklets to achieve temporal alignment and association with the detection. (2) Update the matched tracklets with the corresponding observations, preparing prior information for downstream. Nevertheless, the real-time challenge emerges when managing numerous tracklets, as the filter involves heavy matrix operations on each tracklet. Therefore, we decouple and filter time-invariant states using a lightweight filter to alleviate the computational burden.

Association. As the core of the system, this module establishes tracklet-observation similarity and resolves matching correspondence. Geometry-based (IoU [10], [11], GIoU [1], [2], [4], Euclidean [3], [12], [13], [15], NN distance [5]–[7], [16], etc.) and appearance-based are the commonly used affinity metrics. The former modeling process, reliant solely on spatial information, is mostly unsupervised and robust to occlusion. The latter, robust to inaccurate depth, can describe distant objects. Under the one-to-one assumption, the optimal assignment [33] algorithm is then used to obtain matching pairs. However, rotation in 3D space impairs the parallelization of IoU-like metrics, introducing severe latency. Fast-Poly proposes to leverage alignment to solve this dilemma.

Lifecycle. This module initializes, terminates, and merges tracklets based on the count-based strategy [1]–[4], [10]–[12] or the confidence-based [1], [4], [13], [15] strategy. The former has simple logic and strong robustness. The latter is more flexible in processing based on heuristic functions. In response to the inherent rigidity issue of the former approach, we employ score refinement to flexibly terminate trajectories. In addition, we leverage trajectory average scores and a novel prediction to bolster occlusion robustness and enhance the estimation accuracy of the confidence-based strategy.

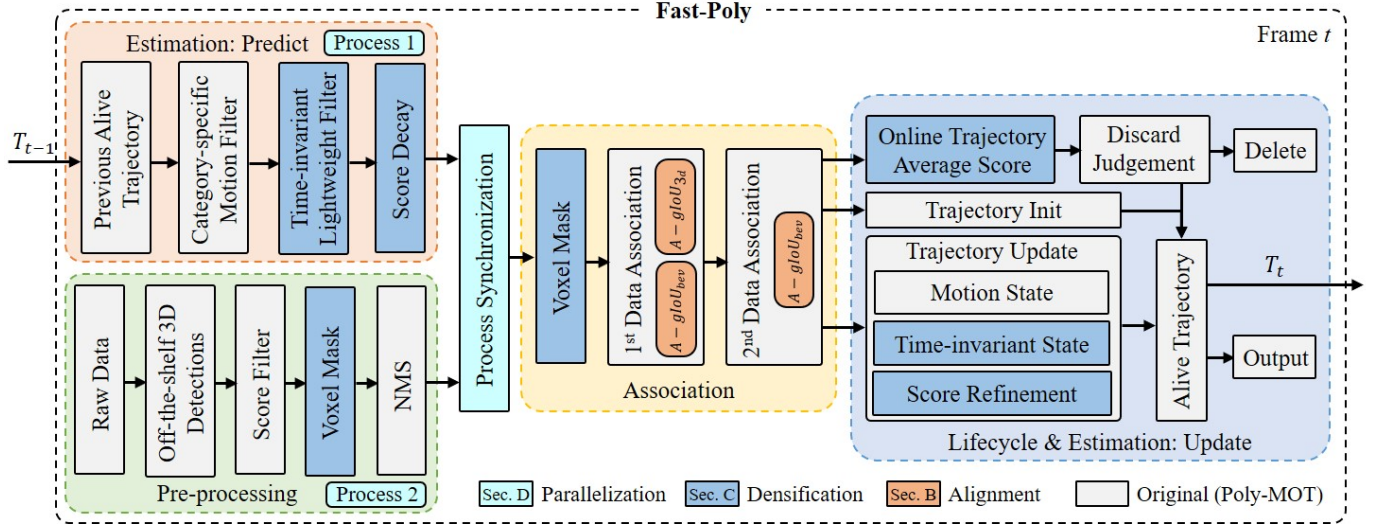


Fig. 2: The pipeline of our proposed method Fast-Poly. Our structure design is illustrated in Section III-A. Real-time improvements to the baseline [1] are highlighted in distinct colors. **Orange** denotes the alignment to counter object rotation. **Blue** denotes the densification to increase computational efficiency. **Cyan** denotes the parallelization to alleviating serial bottleneck.

III. FAST-POLY

A. Overall Architecture

Despite sharing a similar pipeline, Fig. 2 illustrates the distinctions between our proposed method and Poly-MOT [1]. At each frame t , Fast-Poly employs two independent computing processes (Section III-D) to filter the 3D detections D_t and predict existing trajectories $T_{t,t-1}$. Specifically, SF and NMS filters are leveraged to process the detections. Besides, the motion (time-variable), score (Section III-C), and time-invariant (Section III-C) states of trajectories are predicted by corresponding filters. D_t and $T_{t,t-1}$ are then subjected to construct cost matrices C_t^1, C_t^2 for two-stage association. Notably, during NMS and matching, our proposed voxel mask (Section III-C) and a novel geometry-based metric (Section III-B) accelerate computing. Hungarian algorithm [33] is then employed to obtain matched pairs DT_t , unmatched detections D_t^{um} , unmatched tracklets T_{t-1}^{um} . To relieve the matrix dimension, time-invariant and time-variable states in matched tracklets T_{t-1}^m are updated with corresponding observations D_t^m based on our proposed lightweight filter (Section III-C) and Extended Kalman Filter (EKF), respectively. T_{t-1}^m scores are also refined leveraging the confidence-count mixed lifecycle (Section III-C). D_t^{um} are then initialized as newly active tracklets. To flexibly determine FP existing agents in T_{t-1}^{um} , we soft-terminate the mismatch tracklets by considering both their max-age and their online average refined scores. The remaining tracklets T_t are sent to downstream tasks and implemented for next frame tracking.

B. Alignment

In this section, we provide a comprehensive explanation of how Fast-Poly effectively addresses high latency caused by object rotations through alignment, covering both implementation and underlying principles.

GIoU. Without loss of generality, we optimize the widely employed metric in nuScenes SOTA trackers [1], [2] Generalized Intersection over Union $gIoU$, which is formulated as:

$$gIoU(B_i, B_j) = \frac{\Lambda(B_i \cap B_j)}{\Lambda(B_i \cup B_j)} + \frac{\Lambda(B_i \cup B_j)}{\Lambda_{Hull}(B_i, B_j)} - 1, \quad (1)$$

where B is the 3D bounding box representing the detection or tracklet. According to the representation space, $\Lambda(\cdot)$ is the area function in the BEV space and the volume function in the 3D space. $B_i \cap B_j$, $B_i \cup B_j$ and Λ_{Hull} are the intersection, union and convex hull computed by B_i and B_j , respectively.

A-GIoU. Varied from the pixel plane, the rotation causes overlap and convex hull irregular polygons instead of axis-aligned rectangles. The complexity of the well-known Sutherland-Hodgman [34] and Graham scan [35] algorithm are $\mathcal{O}(n^2)$ and $\mathcal{O}(n \log n)$, where n is the number of input points. In addition, the sum calculation time increases rapidly with the growth of detections and tracklets. On the contrary, the solution complexity of the axis-aligned bounding box is only $\mathcal{O}(1)$. To this end, we proposed the Aligned Generalized Intersection over Union ($A-gIoU$), which is formulated as:

$$A-gIoU(B_i, B_j) = \frac{\Lambda(B_i^A \cap B_j^A)}{\Lambda(B_i^A \cup B_j^A)} + \frac{\Lambda(B_i^A \cup B_j^A)}{\Lambda_{Hull}(B_i^A, B_j^A)} - 1, \quad (2)$$

where B^A represents the axis-aligned B , specially containing the top-left and bottom-right points $p \in \mathbb{R}^{1 \times 4}$ on the ground plane. Using the BEV space as a case study, the alignment procedure is depicted in Fig. 3. The overlap and convex hull calculations in Eq. (2) are consistent with $gIoU_{2d}$ [36], with $\mathcal{O}(1)$ computational complexity.

Naturally, two critical questions arise: (1) Can $A-gIoU$ effectively capture inter-object similarity? Our answer is **affirmative**. As demonstrated in Tables VI and II, on nuScenes, integrating $A-gIoU$ in association reduces latency by 73%, while even enhancing accuracy (+0.5% MOTA). Furthermore, (2) why does it perform well in the tracking task? From a

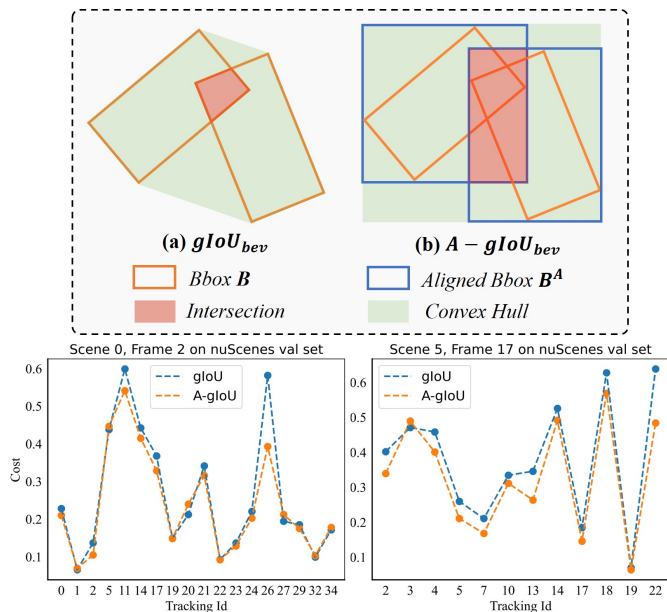


Fig. 3: **Top**: the calculation process of distinct metrics in the BEV space. **Bottom**: the similarity of matched pair between the identical trajectory and detection across two random frames using original $gIoU$ and our proposed $A-gIoU$.

single tracklet or detection perspective, due to the symmetry [36] of $gIoU$, the orientation error between B^A and B is $\leq 45^\circ$. The limited angular loss indicates that B^A can still characterize the spatial information of the object. From the perspective of the correlation between detections and tracklets, Fig. 3 demonstrates that the distances of matched pairs remain unchanged (or changed slightly), thereby illustrating how $A-gIoU$ works. Intuitively, the alignment introduces a uniform scale offset on each trajectory and its corresponding observation. Leveraging the size invariance [36] of $gIoU$, this consistent scale shift preserves the final similarity. Consequently, the matched similarity remains notably higher than that of false matches. Such consistency guarantees the Hungarian algorithm produces similar assignment structures compared to $gIoU$.

C. Densification

In this section, we improve the computational efficiency of the 3D tracking system through three key enhancements: softly eliminating the coasted FP tracklets, introducing the voxel mask, and splitting time-invariant states.

Confidence-Count Mixed Lifecycle. The classic count-based lifecycle seriously raises tracker maintenance costs. In contrast, [15] flexibly terminates tracklets by manipulating scores, significantly reducing FP. However, as evidenced in [15] and Table VII, the deletion based on the latest score and the application of minus prediction detrimentally affect mismatch tracklets due to occlusion or FN detections. Towards this, a power function is first implemented to predict the scores smoothly. The refinement is described in two steps as follows:

$$\begin{cases} \text{Predict: } s_{t,t-1} = \sigma \cdot s_{t-1}, \\ \text{Update: } s_t = 1 - (1 - s_{t,t-1}) \cdot (1 - c_t), \end{cases} \quad (3)$$

where s_{t-1} , $s_{t,t-1}$ and s_t are the $t-1$ frame posterior score, t frame priori score and t frame posterior score of current

tracklet, respectively. c_t is the corresponding detection score. σ is the hand-crafted decay rate, empirically ≤ 0.7 . The update function is similar with [15], satisfies that s_t is more confidence than $s_{t,t-1}$ or c_t . After refinement, tracklets are terminated if their online average scores (computed from the initial frame to the current frame) fall below the deletion threshold θ_{dl} or if the number of mismatch frames exceeds the max-age. There are two noteworthy benefits: (1) Tracklets demonstrate increased resilience to temporary occlusions since their average confidence score decays gradually, as depicted in Table VII. (2) The power function swiftly pulls the tracklet predict score to the $[0, \sigma]$ interval, leaving the over-confidence area ($[0.7, 1]$ interval in Fig. 2 of [15]). This reduces the hysteresis in score estimates, improving the tracking performance.

Voxel Mask. In 3D MOT, an overlooked consideration is: *redundancy and matching are improbable between objects separated by significant distances in 3D Euclidean space*. This stands in stark contrast to inherently no-depth 2D MOT [14], [21], [22]. To address this issue, we propose the voxel mask inspired by the coarse-to-fine idea [37], [38]. Specifically, before computing the global cost based on Eq. (2), i.e., data association and NMS iteration, we employ low-overhead Euclidean distance (2-norm) $\|\cdot\|_2$ and hand-crafted size θ_{vm} to generate voxel mask. The process can be expressed as:

$$\begin{cases} \text{Coarse: } M_t = (\|\mathcal{B}_1^{xyz} - \mathcal{B}_2^{xyz}\|_2 \leq \theta_{vm}), \\ \text{Fine: } C_t = 1 - \text{Aff}(M_t, \mathcal{B}_1, \mathcal{B}_2), \end{cases} \quad (4)$$

where \mathcal{B} is the 3D bounding boxes set representing detections or tracklets based on module representation. \mathcal{B}^{xyz} are the 3D center positions. M_t is the voxel mask between \mathcal{B}_1 and \mathcal{B}_2 . $\text{Aff}(\cdot)$ is the affinity function, i.e., Eq. (2) for association and IoU_{bev} for pre-processing in Fast-Poly. Notably, $\text{Aff}(\cdot)$ directly pads invalid values into false index within M_t to expedite, ultimately yielding C_t .

Lightweight Filter. Current 3D MOT methods embed the time-invariant state (z-position z , width w , length l , height h) of trajectory into the Kalman Filter. However, the time invariance makes the Jacobian matrices of process and observation identity matrices, resulting in numerous meaningless 0-related calculations. Besides, the computational time escalates swiftly with an expanding number of trajectories. To this end, we decouple these states X^{ti} from the KF and estimate them using a compact filter. The estimate process is expressed as:

$$\begin{cases} \text{Predict: } X_{t,t-1}^{ti} = X_{t-1}^{ti}, \\ \text{Update: } X_t^{ti} = \text{LW-Filter}(X_{t,t-1}^{ti}, D_t^i), \end{cases} \quad (5)$$

where X_{t-1}^{ti} , $X_{t,t-1}^{ti}$ and X_t^{ti} are the $t-1$ frame posterior X^{ti} , t frame priori X^{ti} and t frame posterior X^{ti} of current tracklet, respectively. D_t^i is the corresponding detection. $\text{LW-Filter}(\cdot)$ is the custom lightweight filter, implemented by a median or mean filter with length l_{lw} . There are two key insights: (1) $\text{LW-Filter}(\cdot)$ efficiently circumvents invalid computations, facilitating rapid filtering while preserving temporal information. (2) In contrast to KF, which entails manual process and observation noise, $\text{LW-Filter}(\cdot)$ relies solely on a single hyperparameter l_{lw} , reducing overfitting and ensuring robustness, as proven in Fig. 5.

Algorithm 1: Pseudo-code of Parallelization

Input: Current 3D raw detections D'_t ; Previous alive trajectories T_{t-1} ; Frame number N_f

Output: Alive trajectories at current frame T_t

- 1 Initialization: Two parallel processes P_1, P_2 ; Shared flag $Flag = 1$; Shared variables $V = \emptyset$
- 2 # Process P_1 : Pre-processing raw detections of each frame t
- 3 **for** $t \leftarrow 0$ **to** N_f **do**
- 4 **wait** $Flag == 1$ **then**
- 5 $D_t \leftarrow \text{Pre-processing}(D'_t)$
- 6 $V \leftarrow D_t$; $Flag \leftarrow 0$
- 7 **end**
- 8 **end**
- 9 # Process P_2 : Predict trajectories and implement online tracking
- 10 **for** $t \leftarrow 0$ **to** N_f **do**
- 11 $T_{t,t-1} \leftarrow \text{Predict}(T_{t-1})$
- 12 **wait** $Flag == 0$ **then**
- 13 $T_t \leftarrow \text{Tracking}(T_{t,t-1}, V(D_t))$
- 14 $V \leftarrow \emptyset$; $Flag \leftarrow 1$
- 15 **end**
- 16 **end**
- 17 Return: $T_t, t = 0, 1, \dots, N_f$

D. Parallelization

Although the TBD framework is inherently serial, certain modules within it can be parallelized. Consequently, in Fast-Poly, following the tracking in the previous frame, the prediction in the estimation module and the preprocessing module are synchronized in time based on the multi-processing technology. This process is provided as a pseudo-code in Algorithm 1. Specifically, before the online tracking, two parallel processes P_1, P_2 are initiated. This initialization is also accompanied by a shared flag $Flag$ and variable V to synchronize status and transmit data between processes. At each frame t , P_1 filters raw detections while P_2 concurrently predicts the previous alive trajectory and implements online tracking. P_1 and the prediction part of P_2 enter a sleep state after completing their respective tasks, remaining dormant until they are simultaneously awakened in the subsequent frame following the completion of current frame tracking. Our approach adheres to online tracking principles, distinguishing itself fundamentally from [4], which employs multi-processing for synchronous multi-scene tracking.

IV. EXPERIMENTS**A. Dataset and Implementation Details**

nuScenes. nuScenes [8] provides intricate scenes and numerous short sequences (40 frames) with 2Hz for keyframe data. Evaluation encompasses 7 categories: Car (*Car*), Bicycle (*Bic*), Motorcycle (*Moto*), Pedestrian (*Ped*), Bus (*Bus*), Trailer (*Tra*), and Truck (*Tru*). The primary evaluation metric is AMOTA [10]. Fast-Poly is conducted utilizing only keyframes.

Waymo. Waymo [9] provides extended sequences (approximately 20 seconds each) for tracking Vehicle (*Veh*), Cyclist (*Cyc*), and Pedestrian (*Ped*), captured at a frequency of 10Hz. The main evaluation metric, MOTA [23], is categorized into two levels based on the LiDAR points in labels: LEVEL_1 and LEVEL_2. MOTA on LEVEL_2 is reported due to the cumulative nature of difficulty levels.

Implementation Details. Under Python implementation with NumPy [39], Fast-Poly is deployed and tested. We perform the linear search to refine the optimal AMOTA

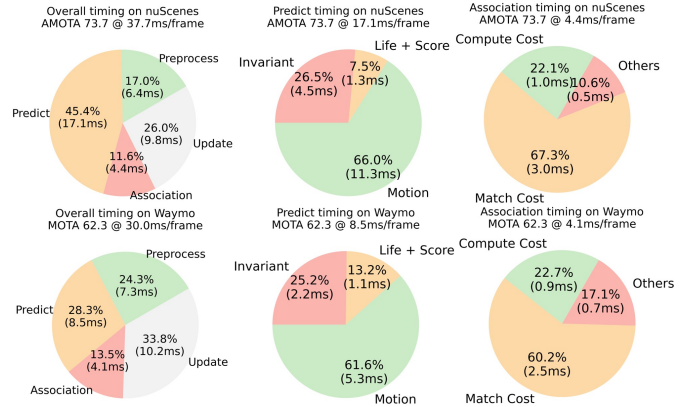


Fig. 4: The average timing statistics of each module in Fast-Poly on the nuScenes and Waymo val set without parallelization. **Invariant** means the lightweight filter for time-invariant states. **Motion** means the Kalman Filter for motion states. **Life** means the lifecycle module. **Score** means the score refinement.

(nuScenes) and MOTA (Waymo) hyperparameters on the validation set. The best hyperparameters are subsequently utilized on the test set. SF thresholds are category-specific and detector-specific, which are (*Moto, Car, Bic*: 0.16; *Bus, Tra*: 0.13; *Tru*: 0; *Ped*: 0.19) on nuScenes, (*Veh*: 0.8; *Ped*: 0.3; *Cyc*: 0.84) on Waymo. The NMS thresholds are 0.08 on all categories and datasets. With default IoU_{bev} in NMS, we additionally utilize our proposed $A-gIoU_{bev}$ to describe similarity for (*Bic, Ped, Bus, Tra*) on nuScenes, (*Veh, Ped, Cyc*) on Waymo. The motion models and filters are consistent with [1]. The lightweight filter is implemented by the median filter with $l_{lw} = 3$ on all datasets. The association metrics are all implemented by $A-gIoU$ on all datasets. The first association thresholds θ_{fm} are category-specific, which are (*Bic, Moto*: 1.6; *Bus, Car, Tra, Tru*: 1.2; *Ped*: 1.8) on nuScenes, (*Veh*: 1.1; *Ped*: 1.3; *Cyc*: 1.2) on Waymo. Voxel mask size θ_{vm} is $3m$ on nuScenes and $5m$ on Waymo. The count-based and output file strategies are consistent with [1]. In the confidence-based part, decay rates σ are category-specific, which are (*Moto, Ped*: 0.6; *Car, Tra, Tru*: 0.2; *Bus*: 0.3; *Bic*: 0.1) on nuScenes, (*Veh*: 0.6; *Ped*: 0.7; *Cyc*: 0.1) on Waymo. The delete threshold θ_{dl} are (*Bus, Ped*: 0.1 and 0.04 for other categories) on nuScenes, (*Cyc*: 0.2; *Veh, Ped*: 0.1) on Waymo.

Metrics. We present four primary indicators: MOTA [23], AMOTA [10], HOTA [24], and FPS (Frame Per Second), supplemented by three secondary indicators: IDS (ID Switch), FP, and FN. The latency of each experiment is the average time cost under multiple evaluations.

B. Run-time Discussion

The comparison with other methods. As shown in Tables I and IV, our inference speed is extremely competitive on both datasets. We outline the detailed time consumption of each module in Figure 4 and Table II. On nuScenes, Fast-Poly can run at 34.2 FPS without any GPU. Besides, the association timing is significantly reduced to 4.4ms, which accounts for only 4% of the original $gIoU$ calculation time. Due to the higher-quality detections (due to the differing requirements between MOTA and AMOTA), the overall timing (35.5 FPS)

TABLE I: A comparison between our proposed method with other advanced methods on the nuScenes test set. This leaderboard is available at [nuScenes official benchmark](#). ‡ means the GPU device. The reported runtimes of all methods exclude the detection time. Fast-Poly and Poly-MOT [1] rely entirely on the detector input, as they do not utilize any visual or deep features.

Method	Device	Detector	Input	AMOTA↑	MOTA↑	FPS↑	IDS↓	FN↓	FP↓
EagerMOT [3]	–	CenterPoint [20]&Cascade R-CNN [40]	2D+3D	67.7	56.8	4	1156	24925	17705
CBMOT [15]	I7-9700	CenterPoint [20]&CenterTrack [22]	2D+3D	67.6	53.9	80.5	709	22828	21604
Minkowski [5]	TITAN‡	Minkowski [5]	3D	69.8	57.8	3.5	325	21200	19340
ByteTrackv2 [17]	–	TransFusion-L [41]	3D	70.1	58	–	488	21836	18682
3DMOTFormer [16]	2080Ti‡	BEVFusion [26]	2D+3D	72.5	60.9	54.7	593	20996	17530
CAMO-MOT [2]	3090Ti‡	BEVFusion [26]&FocalsConv [27]	2D+3D	75.3	63.5	–	324	18192	17269
Poly-MOT [1]	9940X	LargeKernel3D [28]	2D+3D	75.4	62.1	3	292	17956	19673
Fast-Poly (Ours)	7945HX	LargeKernel3D [28]	2D+3D	75.8	62.8	34.2	326	18415	17098

TABLE II: A comparison of the average time consumption of each step of GIoU and our proposed metric A-GIoU in data association on nuScenes val set. **Overlap** means solving intersections. **Convex** means solving convex hulls.

Metric	Overall	Overlap	Convex	Others
<i>gIoU</i>	111.3ms	24.7ms	83.0ms	3.6ms
<i>A-gIoU</i>	0.0098ms	0.0033ms	0.0016ms	0.0049ms

TABLE III: A comparison of the real-time performance on different devices on nuScenes val set with CenterPoint.

Device	Level	FPS↑	AMOTA↑	MOTA↑
Ryzen9 7945HX	Personal	28.9		
Intel 9940X	Server	13.4	73.7	63.2
Cortex A78AE	Embedded	8.7		

as well as that of each module is further reduced for the Waymo dataset. The estimation module dominates the latency, constituting 60% of the total, largely due to the computational demands of solving the Jacobian matrix in the EKF.

The robustness of device migration. As demonstrated in Table III, we evaluated Fast-Poly across three CPU tiers. Since our method is learning-free, tracking accuracy remains unaffected by device migration. On the personal-level CPU, Fast-Poly exhibits the best real-time performance. Besides, considering the challenging outdoor sequences of nuScenes, the inference speed (9 FPS) on Jetson Orin AGX enables its deployment in practical robotic systems.

The parallel efficiency of Fast-Poly. As depicted in Fig. 1, as the number of objects increases significantly, the average frame timing of Fast-Poly exhibits minimal increments (≤ 30 ms). This observation highlights the outstanding computational efficiency and feasibility of our method in autonomous driving scenarios.

C. Comparative Evaluation

nuScenes. Fast-Poly establishes a new state-of-the-art performance on the test set, with 75.8% AMOTA and 34.2 FPS, surpassing all existing methods. With the same detector, Fast-Poly outperforms Poly-MOT [1] on all major metrics (accuracy: +0.4% AMOTA and +0.7% MOTA, latency: +31.2 FPS). Despite being marginally slower than CBMOT [15] and 3DMOTFormer [16] in speed, Fast-Poly significantly outperforms them in accuracy. On a limited computing platform (only personal CPU), Fast-Poly maintains high accuracy

TABLE IV: A comparison between our proposed method with other advanced methods on the Waymo val and test set. The leaderboard is available at [Waymo official benchmark](#). The inference speed is 35.5 FPS.

Split	Method	Detector	Input	MOTA↑
Val	CenterPoint [20]	CenterPoint [20]	3D	55.8
	SimpleTrack [4]	CenterPoint [20]		56.9
	CasTrack [42]	CasA [29]		61.3
	Fast-Poly (Ours)	CasA [29]		62.3
Test	PVRCNN-KF [30]	PVRCNN [30]	3D	55.5
	CenterPoint [20]	CenterPoint [20]		58.7
	SimpleTrack [4]	CenterPoint [20]		60.2
	CasTrack [42]	CasA [29]		62.6
	Fast-Poly (Ours)	CasA [29]		63.6

TABLE V: A comparison between our proposed method with other advanced methods on the nuScenes val set. ‡ means the GPU device. All metrics in the competition papers are reported. Methods in lines 1-7 and lines 8-9 use CenterPoint [20] and LargeKernel3D-L [28], respectively.

Method	Device	AMOTA↑	MOTA↑	FPS↑	IDS↓
OGR3MOT [7]	TITANXp‡	69.3	60.2	12.3	262
SimpleTrack [4]	9940X	69.6	60.2	0.5	405
3DMOTFormer [16]	2080Ti‡	71.2	60.7	54.7	341
ByteTrackv2 [17]	–	72.4	62.4	–	183
ShaSTA [6]	A100‡	72.8	–	10.0	–
Poly-MOT [1]	7945HX	73.1	61.9	5.6	232
Fast-Poly (Ours)	7945HX	73.7	63.2	28.9	414
Poly-MOT [1]	7945HX	75.2	54.1	8.6	252
Fast-Poly (Ours)	7945HX	76.0	65.8	34.2	307

and high real-time consistency. Our method is open-sourced, serving as a strong baseline for 3D MOT.

On the val set, we employ CenterPoint [20] as the detector for a fair comparison. As shown in Table V, Fast-Poly outperforms most learning-based/free methods by a significant margin in terms of both tracking accuracy (73.7% AMOTA, 64.2% MOTA) and latency (29 FPS). We surpass the baseline [1] with a notable improvement of +1.3% in MOTA and +0.6% in AMOTA accuracy, while 5× faster under identical settings. With a powerful detector LargeKernel3D [28], Fast-Poly exhibits stronger tracking performance.

Waymo. As shown in Table IV, with the same detector, we exceed CasTrack [13] with a +1% improvement in MOTA on both test and val sets, showcasing superior tracking performance. Besides, without using the state-of-the-art detector, Fast-Poly ranks 4th on the Waymo tracking leaderboard among all LiDAR-only online methods with 63.6% MOTA to date.

TABLE VI: The ablation studies of each module on the nuScenes val. **AG** means A-GIoU. **VM** means Voxel Mask. **LW** means LightWeight Filter. **CL** means Confidence-Count Mixed Lifecycle. **MP** means Multi-Processing.

Index	Alignment				Densification		Parallelization		Primarily Metric			Secondary Metric		
	AG	VM	LW	CL	MP	AMOTA↑	MOTA↑	FPS↑	IDS↓	FP↓	FN↓			
Baseline [1]	–	–	–	–	–	73.1	61.9	5.6 (188.7ms)	232	13051	17593			
Exp1	✓	–	–	–	–	73.1	62.4	19.9 (50.3ms)	342	13955	16794			
Exp2	✓	✓	–	–	–	73.3	63.0	21.3 (46.9ms)	385	12732	17909			
Exp3	✓	✓	✓	–	–	73.3	62.9	21.7 (46.1ms)	427	14124	16523			
Exp4	✓	✓	✓	✓	–	73.7	63.2	26.5 (37.7ms)	414	14713	15900			
Exp5	✓	✓	✓	✓	✓	73.7	63.2	28.9 (34.6ms)	414	14713	15900			

TABLE VII: A comparison on distinct lifecycle modules on nuScenes val set. **Average** means using the online average score to delete. **Latest** means using the latest score to delete. **Max-age** means using the continuous mismatch time to delete. Other settings are under the best performance.

Strategy	AMOTA↑	MOTA↑	FPS↑	FN↓
Count & Max-age	73.3	62.9	23.0	16523
Confidence [15] & Latest	70.6	63.2	45.8	19192
Confidence [15] & Average	73.3	63.1	28.3	16826
Confidence (Ours) & Average	73.7	63.2	28.9	15900

Despite the scarcity of methods showcasing real-time performance on Waymo, we believe that our inference speed (35.5 FPS) is competitive.

D. Ablation Studies

To verify the effectiveness of each module, we conducted comprehensive ablation experiments on the nuScenes val set. Our baseline tracker Poly-MOT [1] is re-implemented with the official code. With baseline detector CenterPoint [20], the best performance for each ablation experiment is reported.

The effect of the Proposed Metric A-GIoU. As demonstrated in Tables II and VI, *A-gIoU* results in a significant reduction in latency (-138.4ms), particularly notable during the overlap (-24.7ms) and convex hull (-83ms) calculation phases. Additionally, an intriguing observation arises from Table VI, where *A-gIoU* maintains AMOTA (73.1%) and also enhances MOTA (+0.5%). This enhancement stems from the alignment facilitating association to recall more observations (-799 FN).

The effect of the Voxel Mask. As illustrated in Table VI, the increase in accuracy (+0.2% AMOTA, +0.6% MOTA) and decrease in latency (-3.4ms) verify that the voxel mask can avoid invalid cost calculations. An important insight is that the voxel mask avoids excessively distant correlations while also limiting the mismatches (-1223 FP).

The effect of the Lightweight Filter. As indicated in Table VI, combing the lightweight filter results in enhancements in real-time performance (-0.8ms). It is worth mentioning that the lightweight filter also has a slight negative impact on accuracy (-0.1% MOTA), due to the increase in FP and IDS.

The effect of the Confidence-Count Mixed Lifecycle. The notable reduction in FN (-623) and the improvement in AMOTA (+0.4%) showcased in Table VI strongly validate the efficacy of our lifecycle module in bolstering the tracker robustness against mismatch scenarios (occlusion, etc.). The decrease in time consumption (-8.4ms) also proves the marked improvement in trajectory quality. As demonstrated in Table

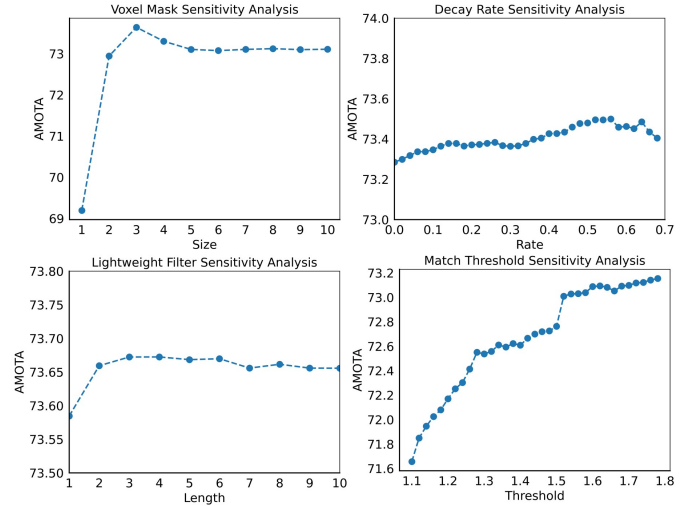


Fig. 5: The comparison of the accuracy under distinct newly introduced hyperparameter. No category-specific technique is performed, all categories are applied the same parameter.

VII, our proposed score refinement exhibits a substantial enhancement in accuracy compared to the original confidence-based method [15], with a noteworthy AMOTA (+3.1%) increase. Besides, the proposed power prediction results in more precise score estimations, thereby contributing to improved accuracy (+0.4% AMOTA, +0.1% MOTA).

The effect of the Parallelization. Without any accuracy loss and without violating the online tracking principle, the multi-processing parallelization effectively alleviates the inherent serial logic of the TBD framework and improves the inference speed by 8.2% (-3.1ms).

E. Hyperparameter Sensitivity Analysis

The plethora of hand-crafted hyperparameters poses a fundamental limitation to the TBD framework. In response, we conduct a sensitivity analysis on newly introduced hyperparameters on the nuScenes val set. Retaining other parameters, the linear search rule is executed for filter length l_{lw} , voxel mask size θ_{vm} , decay rate σ and match threshold θ_{fm} . A critical finding in Fig. 5 is that Fast-Poly showcases insensitivity across all parameters barring θ_{fm} , exhibiting an average fluctuation of less than 0.4% AMOTA. The pronounced decrease in θ_{vm} at 1 stems from erroneous matches induced by artificially narrowing the matching space. Furthermore, θ_{fm} emerges as a pivotal factor for all trackers, manifesting sensitivity across categories [1], [3], [17]. These findings

underscore the resilience of our proposed method in parameter selection. The optimal hyperparameters are delineated in Section IV-A.

V. CONCLUSION

In this work, we proposed an efficient and powerful polyhedral framework for 3D MOT, termed Fast-Poly. To ensure consistency in both accuracy and latency, Fast-Poly integrates three core principles to enhance the baseline Poly-MOT, including: (1) Alignment: By aligning objects, our proposed A-GIoU addresses the detrimental effect of 3D rotation on similarity calculation. (2) Densification: Through soft lifecycle management, voxel mask, and lightweight filter, we enhance the computational efficiency of trajectory maintenance, cost matrix construction, and filter estimation, respectively. (3) Parallelization: Based on multi-processing technology, we perform parallel the prediction and pre-processing modules, effectively alleviating the serial defects of the TBD framework. We conduct extensive experiments on two large-scale tracking benchmarks. Fast-Poly achieves state-of-the-art performance (75.8% AMOTA and 34.2 FPS) among all methods on nuScenes and demonstrates superior real-time and accuracy performance (63.6% MOTA and 35.5 FPS) on Waymo. Fast-Poly is open source and hopes to contribute to the community.

REFERENCES

- [1] X. Li, T. Xie, D. Liu, J. Gao, K. Dai, Z. Jiang, L. Zhao, and K. Wang, "Poly-mot: A polyhedral framework for 3d multi-object tracking," in *IROS*. IEEE, 2023, pp. 9391–9398.
- [2] L. Wang, X. Zhang, W. Qin, X. Li, J. Gao, L. Yang, Z. Li, J. Li, L. Zhu, H. Wang *et al.*, "Camo-mot: Combined appearance-motion optimization for 3d multi-object tracking with camera-lidar fusion," *IEEE T-ITS*, 2023.
- [3] A. Kim, A. Ošep, and L. Leal-Taixé, "Eagermot: 3d multi-object tracking via sensor fusion," in *ICRA*. IEEE, 2021, pp. 11 315–11 321.
- [4] Z. Pang, Z. Li, and N. Wang, "Simpletrack: Understanding and rethinking 3d multi-object tracking," in *ECCV Workshops*. Springer, 2022, pp. 680–696.
- [5] J. Gwak, S. Savarese, and J. Bohg, "Minkowski tracker: A sparse spatio-temporal r-cnn for joint object detection and tracking," *arXiv preprint arXiv:2208.10056*, 2022.
- [6] T. Sadjadpour, J. Li, R. Ambrus, and J. Bohg, "Shasta: Modeling shape and spatio-temporal affinities for 3d multi-object tracking," *IEEE RA-L*, 2023.
- [7] J.-N. Zaech, A. Liniger, D. Dai, M. Danelljan, and L. Van Gool, "Learnable online graph representations for 3d multi-object tracking," *IEEE RA-L*, vol. 7, no. 2, pp. 5103–5110, 2022.
- [8] H. Caesar, V. Bankiti, A. H. Lang, S. Vora, V. E. Liong, Q. Xu, A. Krishnan, Y. Pan, G. Baldan, and O. Beijbom, "nuscenes: A multimodal dataset for autonomous driving," in *CVPR*, 2020, pp. 11 621–11 631.
- [9] P. Sun, H. Kretschmar, X. Dotiwalla, A. Chouard, V. Patnaik, P. Tsui, J. Guo, Y. Zhou, Y. Chai, B. Caine *et al.*, "Scalability in perception for autonomous driving: Waymo open dataset," in *CVPR*, 2020, pp. 2446–2454.
- [10] X. Weng, J. Wang, D. Held, and K. Kitani, "3d multi-object tracking: A baseline and new evaluation metrics," in *IROS*. IEEE, 2020, pp. 10 359–10 366.
- [11] X. Wang, C. Fu, Z. Li, Y. Lai, and J. He, "Deepfusionmot: A 3d multi-object tracking framework based on camera-lidar fusion with deep association," *IEEE RA-L*, vol. 7, no. 3, pp. 8260–8267, 2022.
- [12] H.-k. Chiu, J. Li, R. Ambrus, and J. Bohg, "Probabilistic 3d multi-modal, multi-object tracking for autonomous driving," *ICRA*, 2021.
- [13] H. Wu, W. Han, C. Wen, X. Li, and C. Wang, "3d multi-object tracking in point clouds based on prediction confidence-guided data association," *IEEE T-ITS*, vol. 23, no. 6, pp. 5668–5677, 2021.
- [14] C. Liu, H. Li, and Z. Wang, "Fasttrack: A highly efficient and generic gpu-based multi-object tracking method with parallel kalman filter," *IJCV*, pp. 1–21, 2023.
- [15] N. Benbarka, J. Schröder, and A. Zell, "Score refinement for confidence-based 3d multi-object tracking," in *IROS*. IEEE, 2021, pp. 8083–8090.
- [16] S. Ding, E. Rehder, L. Schneider, M. Cordts, and J. Gall, "3dmtotformer: Graph transformer for online 3d multi-object tracking," in *ICCV*, 2023, pp. 9784–9794.
- [17] Y. Zhang, X. Wang, X. Ye, W. Zhang, J. Lu, X. Tan, E. Ding, P. Sun, and J. Wang, "Bytetrackv2: 2d and 3d multi-object tracking by associating every detection box," 2023.
- [18] T. Zhang, X. Chen, Y. Wang, Y. Wang, and H. Zhao, "Mutr3d: A multi-camera tracking framework via 3d-to-2d queries," in *CVPR*, 2022, pp. 4537–4546.
- [19] Z. Pang, J. Li, P. Tokmakov, D. Chen, S. Zagoruyko, and Y.-X. Wang, "Standing between past and future: Spatio-temporal modeling for multi-camera 3d multi-object tracking," in *CVPR*, 2023, pp. 17 928–17 938.
- [20] T. Yin, X. Zhou, and P. Krahenbuhl, "Center-based 3d object detection and tracking," in *CVPR*, 2021, pp. 11 784–11 793.
- [21] Y. Zhang, P. Sun, Y. Jiang, D. Yu, F. Weng, Z. Yuan, P. Luo, W. Liu, and X. Wang, "Bytetrack: Multi-object tracking by associating every detection box," in *ECCV*. Springer, 2022, pp. 1–21.
- [22] X. Zhou, V. Koltun, and P. Krähenbühl, "Tracking objects as points," in *European conference on computer vision*. Springer, 2020, pp. 474–490.
- [23] K. Bernardin, A. Elbs, and R. Stiefelhagen, "Multiple object tracking performance metrics and evaluation in a smart room environment," in *Sixth IEEE International Workshop on Visual Surveillance, in conjunction with ECCV*, vol. 90, no. 91. Citeseer, 2006.
- [24] J. Luiten, A. Osep, P. Dendorfer, P. Torr, A. Geiger, L. Leal-Taixé, and B. Leibe, "Hota: A higher order metric for evaluating multi-object tracking," *IJCV*, vol. 129, pp. 548–578, 2021.
- [25] J. Huang, G. Huang, Z. Zhu, Y. Ye, and D. Du, "Bevdet: High-performance multi-camera 3d object detection in bird-eye-view," *arXiv preprint arXiv:2112.11790*, 2021.
- [26] Z. Liu, H. Tang, A. Amini, X. Yang, H. Mao, D. L. Rus, and S. Han, "Bevfusion: Multi-task multi-sensor fusion with unified bird's-eye view representation," in *ICRA*. IEEE, 2023, pp. 2774–2781.
- [27] Y. Chen, Y. Li, X. Zhang, J. Sun, and J. Jia, "Focal sparse convolutional networks for 3d object detection," in *Proceedings of the IEEE/CVF Conference on Computer Vision and Pattern Recognition*, 2022, pp. 5428–5437.
- [28] Y. Chen, J. Liu, X. Qi, X. Zhang, J. Sun, and J. Jia, "Scaling up kernels in 3d cnns," *arXiv preprint arXiv:2206.10555*, 2022.
- [29] H. Wu, J. Deng, C. Wen, X. Li, C. Wang, and J. Li, "Casa: A cascade attention network for 3-d object detection from lidar point clouds," *IEEE T-GRS*, vol. 60, pp. 1–11, 2022.
- [30] S. Shi, C. Guo, L. Jiang, Z. Wang, J. Shi, X. Wang, and H. Li, "Pv-rnn: Point-voxel feature set abstraction for 3d object detection," in *CVPR*, 2020, pp. 10 529–10 538.
- [31] K. Huang and Q. Hao, "Joint multi-object detection and tracking with camera-lidar fusion for autonomous driving," in *IROS*. IEEE, 2021, pp. 6983–6989.
- [32] W. Zhang, H. Zhou, S. Sun, Z. Wang, J. Shi, and C. C. Loy, "Robust multi-modality multi-object tracking," in *ICCV*, October 2019.
- [33] H. W. Kuhn, "The hungarian method for the assignment problem," *Naval research logistics quarterly*, vol. 2, no. 1-2, pp. 83–97, 1955.
- [34] I. E. Sutherland and G. W. Hodgman, "Reentrant polygon clipping," *Communications of the ACM*, vol. 17, no. 1, pp. 32–42, 1974.
- [35] R. L. Graham, "An efficient algorithm for determining the convex hull of a finite planar set," *Info. Proc. Lett.*, vol. 1, pp. 132–133, 1972.
- [36] H. Rezatofoghi, N. Tsoi, J. Gwak, A. Sadeghian, I. Reid, and S. Savarese, "Generalized intersection over union: A metric and a loss for bounding box regression," in *CVPR*, 2019, pp. 658–666.
- [37] J. Sun, Z. Shen, Y. Wang, H. Bao, and X. Zhou, "Loftr: Detector-free local feature matching with transformers," in *CVPR*, 2021, pp. 8922–8931.
- [38] C. Bai, T. Xiao, Y. Chen, H. Wang, F. Zhang, and X. Gao, "Faster-lio: Lightweight tightly coupled lidar-inertial odometry using parallel sparse incremental voxels," *IEEE RA-L*, vol. 7, no. 2, pp. 4861–4868, 2022.
- [39] S. Van Der Walt, S. C. Colbert, and G. Varoquaux, "The numpy array: a structure for efficient numerical computation," *Computing in science & engineering*, vol. 13, no. 2, pp. 22–30, 2011.
- [40] Z. Cai and N. Vasconcelos, "Cascade r-cnn: Delving into high quality object detection," in *CVPR*, 2018, pp. 6154–6162.
- [41] X. Bai, Z. Hu, X. Zhu, Q. Huang, Y. Chen, H. Fu, and C.-L. Tai, "Transfusion: Robust lidar-camera fusion for 3d object detection with transformers," in *CVPR*, 2022, pp. 1090–1099.
- [42] H. Wu, W. Han, C. Wen, X. Li, and C. Wang, "3d multi-object tracking in point clouds based on prediction confidence-guided data association," *IEEE T-ITS*, vol. 23, no. 6, pp. 5668–5677, 2021.